



# HHS Public Access

Author manuscript

*Nat Neurosci.* Author manuscript; available in PMC 2010 July 01.

Published in final edited form as:

*Nat Neurosci.* 2010 January ; 13(1): 133–140. doi:10.1038/nn.2467.

## A robust and high-throughput Cre reporting and characterization system for the whole mouse brain

Linda Madisen<sup>1</sup>, Theresa A. Zwingman<sup>1</sup>, Susan M. Sunkin<sup>1</sup>, Seung Wook Oh<sup>1</sup>, Hatim A. Zariwala<sup>1</sup>, Hong Gu<sup>1</sup>, Lydia L. Ng<sup>1</sup>, Richard D. Palmiter<sup>2</sup>, Michael J. Hawrylycz<sup>1</sup>, Allan R. Jones<sup>1</sup>, Ed S. Lein<sup>1</sup>, and Hongkui Zeng<sup>1,\*</sup>

<sup>1</sup> Allen Institute for Brain Science, Seattle, WA 98103, USA

<sup>2</sup> Howard Hughes Medical Institute, Department of Biochemistry, University of Washington, Seattle, WA 98195, USA

### Abstract

The Cre/lox system is widely used in mice to achieve cell-type-specific gene expression. However, a strong and universal responding system to express genes under Cre control is still lacking. We have generated a set of Cre reporter mice with strong, ubiquitous expression of fluorescent proteins of different spectra. The robust native fluorescence of these reporters enables direct visualization of fine dendritic structures and axonal projections of the labeled neurons, which is useful in mapping neuronal circuitry, imaging and tracking specific cell populations *in vivo*. Using these reporters and a high-throughput *in situ* hybridization platform, we are systematically profiling Cre-directed gene expression throughout the mouse brain in a number of Cre-driver lines, including novel Cre lines targeting different cell types in the cortex. Our expression data are displayed in a public online database to help researchers assess the utility of various Cre-driver lines for cell-type-specific genetic manipulation.

### Introduction

In functional studies of the mouse brain, transgenic lines have played an invaluable role in various strategies including: labeling specific neurons by fluorescent protein expression<sup>1–3</sup>, knocking out or over-expressing genes in specific cell types<sup>4–6</sup>, and ablating or inhibiting activity of specific neuronal populations<sup>7–9</sup>. New molecular tools developed over the last decade have transformed approaches to study neural circuitry and plasticity with exquisite detail and control (reviewed in<sup>10, 11</sup>). For example, use of transgenic mice that express fluorescent markers at relatively high levels in defined neuronal populations, such as *Thy1-*

Users may view, print, copy, download and text and data-mine the content in such documents, for the purposes of academic research, subject always to the full Conditions of use: [http://www.nature.com/authors/editorial\\_policies/license.html#terms](http://www.nature.com/authors/editorial_policies/license.html#terms)

\*Corresponding author. Phone: (206) 548-7104; hongkuiz@alleninstitute.org.

#### Author Contributions

H.Z. designed the study, analyzed data and wrote the paper. L.M. generated the Cre reporter lines and the knock-in Cre driver lines. T.A.Z. and E.S.L. designed and generated the BAC transgenic Cre driver lines. H.Z., S.M.S. and T.A.Z. set up the characterization pipeline and database. S.W.O. produced and performed experiments with rAAVs. H.A.Z. performed *in vivo* 2-photon imaging experiments. M.J.H. and L.L.N. conducted informatics analysis. H.G. assisted with transgenic mice production and characterization. R.D.P. provided lab resources and scientific advice. A.R.J. provided institutional support.

EYFP<sup>1</sup>, has facilitated detailed studies of the properties of a single neuron: morphology, connectivity, electrophysiology and gene expression<sup>2, 12</sup>, and permits long-term *in vivo* imaging<sup>13</sup>. The Brainbow mice introduced a new strategy for simultaneous mapping of projections and connectivity among multiple neurons using multicolored fluorescence<sup>14</sup>. Genetic manipulations that allow one to reversibly activate or silence neurons are powerful new ways to examine neural circuits that underlie behavior and plasticity. Among these, manipulation of neuronal activity on a millisecond scale is achievable by expression of light-gated ion channels such as channelrhodopsin (ChR2)<sup>15</sup>.

However, a significant hurdle for widespread use of ChR2 is that high expression level is required to generate sufficient current to activate target neurons. While this has been achieved using acute approaches that deliver high transgene copy numbers, such as *in utero* electroporation or recombinant viruses, robust ChR2 expression has been difficult to obtain in transgenic mice, with the exception of using the *Thy1* promoter<sup>16</sup>. However, the *Thy1* promoter is sensitive to positional effects when randomly integrated into the genome, has a postnatal onset of expression, and lacks ubiquitous neuronal expression. Similar to ChR2, many other genetic tools would also benefit from a strong and universal transgenic expression platform. One of the most desirable ways to achieve this is to develop universal Cre-responder lines that strongly express fluorescent markers or genetic tools.

To date, the most commonly used locus for generating Cre-responder mice is the *Gt(ROSA)26Sor* (*Rosa26*) locus<sup>17</sup>. However, expression of fluorescent reporters (*e.g.* GFP) directly from the endogenous *Rosa26* promoter<sup>18</sup> is poor in the adult mouse brain. Other Cre-reporter lines using strong promoters but integrated into random loci (*e.g.* Z/EG<sup>19</sup> and Brainbow<sup>14</sup>) are generally not universally expressed. Thus, there remains a significant need for a Cre-dependent system with the potential to confer high-level responder expression in any Cre-defined cell type. Although serving different purposes, the creation of the MADM<sup>3</sup> and mT/mG<sup>20</sup> mice demonstrated a potential approach to achieving higher-level universal expression by incorporating a stronger exogenous promoter into a permissive genomic locus such as *Rosa26*. Furthermore, despite the widespread use of Cre lines and the importance of complete knowledge of where Cre-mediated recombination occurs, the lack of a systematic approach for Cre expression profiling has prevented full characterization of Cre-dependent gene expression patterns in many Cre-driver lines, creating uncertainty in interpretation of results and in selection of appropriate Cre lines for specific research purposes.

Here we report the development of several robust and universal Cre-responder lines that show intense native fluorescent labeling. We further introduce a public database for systematic characterization of Cre recombination patterns in various Cre-driver lines. Characterization data for 21 Cre-driver lines, including 10 newly generated Cre lines that target cortical cell types, are presented. These new Cre lines could be useful tools in the study of cortical circuits and function. Through standardized and detailed anatomical profiling of transgene expression in the entire mouse brain, this dataset provides a comprehensive evaluation of each transgenic mouse line to help researchers choose appropriate transgenic tools for studying the function of specific regions and/or cell types of the brain.

## Results

### Generation of Cre-reporter mice from a universal locus

We utilized the Rosa26 locus<sup>17</sup> to develop a universal Cre-responder because Rosa26 is a ubiquitous locus that also permits an exogenous strong promoter inserted within it to drive higher expression<sup>3, 20</sup>. The Rosa26 locus was modified by targeted insertion of a construct containing the strong and ubiquitous CAG promoter, followed by a floxed-Stop cassette-controlled fluorescent marker gene (Fig. 1a). Four lines (Fig. 1b) were generated with similar components but different fluorescent proteins: EYFP, ZsGreen or tdTomato. ZsGreen and tdTomato are among the brightest fluorescent proteins currently available<sup>21</sup>. The woodchuck hepatitis virus posttranscriptional regulatory element (WPRE)<sup>22</sup> was used in all but the Ai2 line to enhance mRNA transcript stability. Using the pair of PhiC31 recognition sites, AttB/AttP, the PGK-Neo marker can be deleted from the reporter lines in either ES cells or mice (Supplementary Fig. 2 online). This was done for the Ai9 line by transfecting Ai9 ES cells with a PhiC31-expressing plasmid<sup>23</sup> to produce the -Neo line, Ai14 (Fig. 1b). Removal of the Stop cassette by Cre transfection showed that both ZsGreen and tdTomato produce brighter fluorescence than EYFP in ES cells (Supplementary Fig. 3 online). In addition, a pair of FRT sites was incorporated to allow for a FLP recombinase-mediated replacement strategy (“Flp-in”) to swap other genes into the same locus at high efficiency (>90%) using a double-selection strategy (Supplementary Fig. 4 online).

### Strong fluorescent labeling of various brain cell types

The new reporter lines were bred with various Cre lines (Table 1) to test expression of the reporter genes and compare with the existing Rosa26-EYFP line<sup>18</sup>. In a direct comparison at mRNA level by ISH of Cre-activated reporter gene expression in the cortex (Fig. 1c), the Rosa26-EYFP reporter line showed weak EYFP signal throughout the cortex. The Ai2 line had enhanced EYFP expression compared to Rosa-EYFP, albeit a still moderate level. The Ai3, Ai6 and Ai9 lines showed similarly strong expression of the reporter genes; reporter expression at the single-cell level in these lines was found to approach closer to that present in the strongly expressing *Thy1*-EYFP mice<sup>1</sup>. Similar results were observed in other brain regions in all other Cre-reporter crosses mentioned in Table 1 (data not shown).

To quantify expression difference in ISH signals for Rosa26-EYFP, Ai2 and Ai3, which all used the same EYFP probe for ISH, relative optical density measured as the Integrated Optical Density (IOD) ratio was computed for each area of interest (AOI) using algorithms developed for the Allen Mouse Brain Atlas<sup>24</sup>. In comparison of mice in which each reporter line was crossed to the ubiquitous EIIa-Cre, with whole brain sections as AOIs (Fig. 1d), the increase of expression levels from Rosa26-EYFP to Ai2 and then to Ai3 is highly significant ( $p < 0.001$  in all pair-wise comparisons). Moreover, quantitative RT-PCR of EYFP (Fig. 1e) was done on the cerebellums of mice in which each reporter line was crossed to Pcp2-Cre, a Cre line that drives Purkinje cell-specific expression in the cerebellum. Amplification of EYFP transcript from Rosa26-EYFP requires significantly more cycles than that from Ai2 or Ai3 (differs by >3 PCR cycles,  $p < 0.001$  in both comparisons), whereas the difference between Ai2 and Ai3 is small (~0.4 PCR cycles) but still significant ( $p = 0.021$ ).

Consistent with the ISH and qPCR results, all reporter lines displayed moderate (in Ai2) to strong (in Ai3, Ai6, Ai9 and Ai14) native fluorescence. In particular, Ai6, Ai9 and Ai14 exhibited bright fluorescence throughout the body (e.g. Supplementary Fig. 5 online) that could greatly facilitate *in vivo* imaging. In the adult brains, when crossed to the same Cre line, different new reporter lines gave similar expression patterns overall with different degrees of fluorescence intensity (Fig. 2a–b), all substantially stronger than Rosa26-EYFP, whose native fluorescence is mostly below detection and requires immunohistochemical (IHC) staining to reveal expression. While the EYFP and tdTomato fluorescence was uniformly distributed throughout the cells and their processes, the Ai6 ZsGreen fluorescence was mostly confined to cell bodies, giving rise to a punctate cellular labeling pattern (Fig. 2a–b and Supplementary Fig. 6 online).

To assess the fluorescence intensity of different fluorescent proteins in a more objective way, TetraSpeck fluorescent beads (4.0  $\mu\text{m}$ ) were spread directly onto sections and used as a standard to compare the brightness of fluorescently labeled cells in different brain sections (Supplementary Fig. 7 online). The assessed strength of native fluorescence increases in the following order: Rosa-EYFP < Ai2 (EYFP) < Ai3 (EYFP) < Ai9 (tdTomato) = Ai14 (tdTomato) < Ai6 (ZsGreen), regardless of which Cre lines were used. Further quantification of fluorescent signals at single cell level (Fig. 2c) was done on sections from mice in which each of Rosa26-EYFP, Ai2 or Ai3 was crossed to *Pcp2*-Cre, which not only induces recombination in Purkinje cells but also partially elsewhere, especially in hippocampus and visual cortex. The cerebellar Purkinje cells, cortical neurons and hippocampal CA1 pyramidal cells all showed significantly stronger labeling by Ai3 than Ai2 ( $p < 0.001$  in all comparisons), and labeling in Rosa26-EYFP was essentially undetectable. Taken together, these data demonstrate that the new reporter lines have enhanced reporter gene expression and there is a further improvement from Ai2 to Ai3. Difference between Ai2 and Ai3 indicates that the WPRE sequence improved transcript and/or protein expression in our system.

With the significantly enhanced reporter expression, more recombined cells than expected from previous reports were readily detected in various Cre-driver lines, such as *Slc6a3*-Cre<sup>25</sup> and *Pcp2*-Cre<sup>26</sup> (Supplementary Fig. 8 online), in which Cre-mediated recombination was previously thought to be limited to certain cell types using Rosa26-LacZ or Rosa26-EYFP reporter mice. These results indicate either that the new reporter lines are more sensitive to low levels of Cre, leading to a more thorough identification of Cre-positive populations, and/or that Cre-mediated recombination had occurred in more cells in previous reporter lines, but it was undetected due to low reporter expression.

Strong tdTomato native fluorescence in Ai9 and Ai14 allowed direct visualization of fine structural details, such as dendritic spines and thin axons, of diverse cell types (excitatory, inhibitory, or glial) under confocal microscopy (Fig. 2d–h). Further, it is possible to use these reporter lines to map long-range axonal projections. For example, breeding Ai14 to the *Ntsr1*-Cre line, known to label cortical layer 6 excitatory neurons<sup>27</sup>, resulted in strong labeling of the corticothalamic projections (Fig. 2i). A Cre-expressing recombinant adeno-associated virus (rAAV-Cre) was also used in conjunction with these reporter lines to map axonal projections. Following rAAV-Cre virus injection into the somatosensory cortex of an

Ai14 mouse, the corticothalamic, corticocollosal, and corticospinal projections were all strongly fluorescent (Fig. 2j and data not shown). Strong tdTomato native fluorescence also enabled direct visualization of cells in live animals by *in vivo* 2-photon imaging, in which tdTomato-positive neurons (red) and calcium dye-loaded neurons (green) were easily distinguishable (Fig. 2k). Dendrites of tdTomato-positive neurons were also clearly visible (as the small red dots).

### Systematic characterization of Cre recombination patterns

Utilizing the systems developed for the generation of the Allen Mouse Brain Atlas (<http://mouse.brain-map.org>)<sup>24</sup>, a characterization pipeline has been developed to systematically evaluate gene expression patterns throughout the entire mouse brain, that are defined by various Cre-driver lines. The pipeline is advantageous in that characterization data are generated on sections covering the entire brain, high resolution images are obtained, ISH data are registered to the Allen Reference Atlas<sup>28</sup> and can be used for informatics data mining, and all characterization data are publicly displayed at <http://transgenicmouse.alleninstitute.org/>.

To date, we have systematically characterized over 20 Cre-driver lines (Table 1). These cover both a representative set of Cre lines previously generated by other researchers for which comprehensive characterization is reported for the first time here, as well as a set of new Cre lines generated by us. The following types of data are included. (1) Colorimetric ISH (CISH) of Cre or the reporter gene shows mRNA expression at single-cell resolution. (2) Double fluorescent *in situ* hybridization (DFISH) of the reporter gene with another gene of interest, either the original targeted gene or another cell-type marker, shows the degree of pattern recapitulation or the cell-type identity. (3) XFP native fluorescence or IHC of the reporter gene shows expression of the reporter gene at the protein level throughout the brain (*e.g.* Fig. 2a–b). A characterization example is shown in Supplementary Figure 9 online for *Chat*-Cre.

Using previously developed algorithms for informatics image processing<sup>29</sup>, the ISH dataset can provide additional information on the localization of gene expression. As an example, we evaluated EYFP expression pattern in the *Slc6a3*-Cre/Ai3 mouse. In *Slc6a3*-Cre<sup>25</sup>, Cre is targeted to the dopamine transporter gene (*Slc6a3*) which is expressed in dopaminergic neurons. Compared with the ISH of *Slc6a3* gene itself, EYFP expression was found to be more widespread, not only present in the dopaminergic neurons, *e.g.* in the ventral tegmental area (VTA)/substantia nigra and co-localized with *Slc6a3* (Fig. 3a, left panel), but also present in other brain regions, mostly sparsely scattered but also clustered in some areas of the basal forebrain (*e.g.* Fig. 3a, right panel), corticoamygdala area, and brainstem (data not shown). Registration of the EYFP ISH data to the Allen Reference Atlas was done (Fig. 3b), in which each section was fit into the 3D reference volume along with detected ISH signals. The expression pattern was further visualized as a 3D model using Brain Explorer<sup>30</sup>, and anatomical partitioning was overlaid onto each section. The nearest Allen Reference Atlas plane was then extracted for each section to assist in the identification of the region of interest. Using this approach, the cluster of EYFP-positive cells seen in the basal forebrain was localized to the bed nuclei of the stria terminalis (BST, Fig. 3b, red arrow). This

prediction is consistent with previous studies indicating that the dopamine transporter might be transiently expressed in BST during development<sup>31</sup>.

### Generation and characterization of new Cre-driver lines

We have generated a set of new Cre-driver lines designed to target different excitatory or inhibitory cell types in the cortex. Analysis of Cre-directed reporter expression and reporter co-localization with *Gad1* in these new Cre lines, along with 2 pre-existing Cre lines (*Six3-Cre*<sup>32</sup> and *Ntsr1-Cre*<sup>27</sup>), is shown in Figure 4 to illustrate diverse cortical Cre-recombination patterns. Specifically, two BAC transgenic Cre lines targeting a layer 2 marker (*Wfs1*), *Wfs1-Tg2-CreERT2* and *Wfs1-Tg3-CreERT2*, drive preferential recombination in layers 2/3 after tamoxifen induction, with somewhat different profiles (Fig. 4a). Two BAC transgenic Cre lines targeting a layer 4 marker (*Scnn1a*) also show specific recombination in layer 4 of varying degrees, with very sparsely labeled layer 4 cells (mostly in the somatosensory cortex) in the *Scnn1a-Tg2-Cre* line and denser layer 4 labeling in the *Scnn1a-Tg3-Cre* line (Fig. 4b). In contrast to these lines in which Cre-recombination more or less follows that of the endogenous targeted genes, the following 2 BAC Cre lines display entirely different patterns from the original genes. The *A930038C07Rik-Tg4-Cre* line displays expression in a sparse population of cells encompassing layers 3/4/5 (Fig. 4d), whereas the endogenous *A930038C07Rik* gene is layer 1 specific. The *8030451F13Rik-Tg2-Cre* line shows expression in a scattered population of cells that are not GABAergic (Fig. 4f), whereas the endogenous *8030451F13Rik* gene expresses in a scattered interneuron population. In other cases, as reported previously, the *Six3-Cre* line drives preferential expression in layer 4 (Fig. 4c), and the *Ntsr1-Cre* line shows specific expression in layer 6 (Fig. 4e). A short (1.3kb) *Camk2a* promoter-driven new Cre line *Camk2a-CreERT2* (Fig. 4g), produced by random integration into the genome, drives “leaky” expression in scattered excitatory neuronal populations in the uninduced state. After tamoxifen induction, expression is seen in the majority of excitatory neurons, consistent with the endogenous *Camk2a* expression pattern. Finally, an *ErbB4-2A-CreERT2* knock-in Cre line (Fig. 4h), in which the 2A-CreERT2 sequence is inserted in frame to the 3' end of the coding sequence (immediately upstream of the stop codon) of *ErbB4*, which is predominantly expressed in interneurons, shows Cre-recombination in a sub-population of GABAergic interneurons in both cortex and hippocampus only after tamoxifen induction. The reporter-labeled cells co-localize with most, but not all, cells that are *ErbB4* positive. Overall, the diversity of recombination directed by these Cre-driver lines constitutes useful tools for the study of different excitatory and inhibitory cortical cell types.

To explore the utility of the 2A sequences<sup>33</sup> in mediating bicistronic translation in a mechanism different from, and potentially more efficient than, the well described IRES (internal ribosome entry site) sequence, we generated a *Pvalb-2A-Cre* knock-in line, in which the 2A-Cre sequence is inserted in frame to the 3' end of the *Pvalb* coding sequence (immediately upstream of the stop codon). The resulting Cre-driver line has a similar genomic configuration as the previously reported *Pvalb-ires-Cre* line<sup>34</sup>, in which *ires-Cre* is inserted by knock-in into the *Pvalb* 3' UTR. A comparison of Ai14 reporter expression in crosses to each of the two *Pvalb* Cre-driver lines is shown in Figure 5. *Pvalb* is a robust marker for a subset of cortical interneurons (e.g. basket cells and chandelier cells), but it is

also expressed at lower levels in other types of cells, *e.g.* some layer 5 pyramidal neurons (Fig. 5b). In thalamus, *Pvalb* is expressed most strongly in the reticular nucleus (RT) and less strongly in other regions, such as the ventral posteromedial nucleus (VPM) (Fig. 5h). We found that in the *Pvalb*-ires-Cre mice, recombination appears to occur only in cells with strongest *Pvalb* expression, *i.e.* those large interneurons, and thus a more restricted (and perhaps more specific) pattern emerges than the *Pvalb* gene itself. On the other hand, in the *Pvalb*-2A-Cre mice, recombination appears more widespread, occurring in cells with both high and low levels of *Pvalb* expression. These results indicate that different recombination patterns may be produced from different targeting methods even in the same locus. An IRES-mediated approach may result in lower Cre protein levels and may be better used in conjunction with strong genes to increase recombination specificity. A 2A-based approach may produce a more equal-molar level of Cre and may be better used with weakly-expressing genes to increase sensitivity. Our data suggest a source of recombination variability beyond the commonly recognized positional effect as seen in the above BAC Cre lines. Also, to our knowledge the *Pvalb*-2A-Cre and *ErbB4*-2A-CreERT2 are the first demonstration that 2A sequences are able to mediate faithful Cre expression when targeted to the endogenous gene loci.

## Discussion

Given the tremendous potential of using transgenic tools to tease out different components of complex neural circuits, great effort has been put into developing a large number of cell-type-specific Cre-driver lines (*e.g.* ref <sup>27</sup>). The field is just beginning to create the necessary number of Cre responsive lines expressing molecular probes or tools. Impeding successful development of useful lines is the requirement for most of these probes/tools to be expressed at sufficiently high levels in order for them to work well *in vivo*; so far, there has not been an optimal way to achieve this expression. Cre-responding recombinant viral vectors can confer strong expression, and they offer a fast, convenient alternative approach<sup>35, 36</sup>. However, variability in different viral stocks, serotypes, injected animals, cell type infection efficiency, number of viral particles present in individual cells, etc. is inherent to the viral approach, and is a major issue in functional studies. Here, we demonstrate success in creating a consistent and versatile system to strongly express fluorescent probes. Importantly, our system should allow us to express various additional functional genes, which in combination with the ever increasing number of Cre mouse lines will expand the arsenal of Cre-controlled tools specific for a variety of cell types.

The expression of exogenous genes at high levels always carries the risk of potential toxicity. So far we have not observed any morphological abnormalities in either the mice or the various cell types examined. Notably, we have created animals of which the floxed-Stop cassette is deleted in germline and the fluorescent reporters are strongly expressed throughout the body. These animals are healthy and fertile with no significant behavioral or anatomical abnormalities. Nonetheless, it will be necessary to continue monitoring for potential subtle phenotypes.

In addition to what we have shown, one can envision more applications in the use of these novel Cre-reporter lines, especially the Ai9/Ai14 tdTomato lines. Upon crossing to different

cell-type-specific Cre lines, one can examine the morphology of labeled cells, trace axonal projections (in a way similar to <sup>37</sup>), record electrophysiological activities, perform short-term and long-term *in vivo* imaging, and follow development and differentiation. Specific cell populations can also be isolated by cell sorting or other means for subsequent gene expression profiling, culturing, or transplantation. Differential fluorescently labeled cell types can be mixed or transplanted together to examine their interactions and formation of microcircuits both *in vitro* and *in vivo*.

Through the systematic analysis of various Cre-driver lines, we observed a wide range of Cre-recombination patterns that can be less than, more than, or different from what is expected. This diversity could be due to positional effect of a randomly integrated Cre-transgene, the level of Cre expression, the accessibility of floxed targets, or early developmental or sporadic, transient expression of Cre. The latter could also be a faithful reflection of the developmental or transient expression of the original targeted gene in previously unknown cell types, thus it could serve to uncover novel functions of the gene. To date, all of our characterizations are in adult mouse brain. It will be useful to expand these characterizations into different developmental stages as well as other tissues. Since Cre-recombination converts dynamic gene expression into a permanent on or off state (of a reporter or a floxed gene), this approach of collecting data in an extensive and standardized way should be valuable in guiding the choice and evaluation of different Cre transgenic tools, as well as future efforts toward using combinatorial strategies to achieve even greater cell-type-specific genetic control.

### Open public access

All research materials and data are publicly available. DNA constructs will be deposited to Addgene, Inc., a plasmid repository, for distribution. New Cre-reporter mice have been deposited to the Jackson Laboratory for distribution (JAX Stock Numbers for Ai2: 007920; Ai3: 007903; Ai6: 007906; Ai9: 007909; Ai14: 007914). Some of the new Cre-driver lines have also been deposited to JAX (see Table 1), and the remaining lines are in the process. Transgenic mice characterization data, as well as detailed experimental protocols, are available at <http://transgenicmouse.alleninstitute.org/>. In the future, we will continue to characterize new Cre-driver lines made by ourselves and from the scientific community, including those that are in the JAX Mice repository. These characterization data will also be publicly available on the web site.

## Methods

### Gene targeting in ES cells and generation of knock-in mice

Targeting constructs were generated using a combined gene synthesis (GenScript Corp.) and molecular cloning approach. Briefly, to target the Rosa26 locus, a cassette containing the following components was constructed: FRT – LoxP – Stop codons – 3x SV40 polyA – LoxP – EYFP – WPRE – bGH polyA – AttB – PGK promoter – FRT – Neo – PGK polyA – AttP. For most targeting vectors, this cassette was cloned into a Rosa-CAG targeting vector<sup>3</sup>, downstream of the CAG promoter and upstream of the 3' arm, to generate the final EYFP targeting vector. Unique restriction sites flanking the EYFP gene were used to replace

EYFP with alternative reporter genes. For the Ai2 vector, which lacks the WPRE, the CAG promoter was inserted between the first FRT and LoxP sites, and the cassette was cloned immediately downstream of the 5' homology arm. The final targeting vectors contained 5' and 3' homology arms of 1.1 kb and 4.3 kb, as well as a PGK-DTA cassette for negative selection. Targeting constructs for knock-in Cre lines inserted into other gene loci were constructed in similar ways.

The targeting vectors were linearized and transfected into the 129/B6 F1 hybrid ES cell line G4<sup>42</sup> using an Amaxa electroporator. G418-resistant ES clones were screened by Southern blot analysis of *HindIII* digested DNA, which was probed with a 1.1 kb genomic fragment from immediately upstream of the 5' arm. We observed a recombination rate of about 25% for the four constructs. Positive ES clones were injected into C57BL/6J blastocysts to obtain chimeric mice following standard procedures. Both ES cell transfections and blastocyst injections were performed by the University of Washington Transgenic Resources Program. Due to the robustness of the G4 cells, high-percentage chimeras and high rates of germline transmission were routinely obtained. Chimeric mice were bred with either C57BL/6J mice to obtain germline transmission or various Cre-driver lines for direct characterization.

An Ai9 ES cell clone with strong germline transmission potency was used in subsequent transfections for the FLP-mediated exchange strategy outlined in Supplementary Figure 4 online. Ai9 ES cells were co-transfected using a Bio-Rad electroporator with 100 µg of pCAGGS-FLPe (Open Biosystems) and 40 µg of an incoming replacement vector. After 8 to 10 days of Hygromycin B selection, surviving colonies that also appeared green by fluorescence microscopy were picked and screened by PCR using primer sets designed to confirm a correct insertion of the incoming vector at the 5' and 3' FRT recombinase sites.

### Generation of BAC transgenic Cre-driver lines

Plasmids containing straight Cre and inducible CreERT2 along with a selectable marker flanked by Frt sites (Frt-Neo-Frt) were utilized for all subsequent targeting to BACs containing genes of interest. The Cre Frt-Neo-Frt portions of the plasmids were PCR amplified with flanking oligos that were designed to have 50bp homology arms with the BAC of interest. Specific BAC clones used are: RP23-476E22 for *A930038C07Rik*, RP23-405O19 for *Wfs1*, RP23-405B24 for *Scnn1a*, and RP23-116K19 for *8030451F13Rik*. RedET recombination<sup>43</sup> was used to insert the sequence verified PCR product into the ATG start site of the specific gene locus on each BAC. FLP recombination was used to remove the neomycin selection marker from the BAC. The wild type loxP site present in the RP23 BAC backbone was removed before pronuclear injection. Plasmid construction was done by Gene Bridges GmbH (Heidelberg, Germany).

BAC DNA for pronuclear injection was prepared using NucleoBond BAC100 kit (Clontech), linearized and purified over a Sepharose CL4b column. Fractions were analyzed by pulse field gel electrophoresis to identify the sample with the highest concentration of linearized BAC DNA and lowest concentration of vector DNA. Linearized BAC DNA was injected at a concentration of 1 ng/µl into C57BL/6 x B6C3F1 zygotes.

## Transgenic mice characterization

All experimental procedures were approved by the Institutional Animal Care and Use Committee (IACUC) of Allen Institute for Brain Science in accordance with NIH guidelines. All characterization was done using adult mice around ages P56 or older. The mice that were characterized were in a mixed genetic background, containing 50–75% C57BL/6 background and the remainders of 129 or other backgrounds from the various Cre lines. For systematic characterization of fluorescent proteins either by their native fluorescence or IHC, perfused brains were cryosectioned using a tape transfer technique, sections were then DAPI stained directly or following antibody staining, and images were captured using automated fluorescent microscopy. Microtome sections of 100- $\mu$ m thickness from perfused brains were used for confocal imaging of fluorescently labeled cells. For systematic characterization of gene expression by colorimetric ISH or DFISH, the Allen Institute established pipelines for tissue processing, probe hybridization, image capture and data processing were utilized. Informatics signal identification, mapping, and quantification used the Allen Mouse Brain Atlas spatial mapping platform<sup>24, 29</sup>. In this pipeline, image series are preprocessed (white-balanced and cropped), then registered to a three-dimensional informatics reference atlas of the C57BL/6J mouse brain<sup>28</sup>. This registration enables data to be displayed in 2D sections or reconstructed 3D volumes.

## Tamoxifen induction

Tamoxifen was prepared by first dissolving in ethanol (20 mg/500  $\mu$ l) and mixing this solution with 980  $\mu$ l corn oil for a final concentration of 20 mg/ml. Ethanol was then removed with a heated speed vacuum. Mice containing CreERT2 that were ~2 months old were injected with approximately 200  $\mu$ l tamoxifen solution (200 mg/kg) once a day over 5 days. Animals were monitored for adverse effects, and if these became apparent, treatment was stopped. One week after treatment ended, animals were processed as described below for ISH or localization of XFP.

## Colorimetric *in situ* hybridization (CISH)

The systems developed for processing tissue, RNA *in situ* hybridization (ISH), Nissl staining, image acquisition, and data processing for the generation of the Allen Mouse Brain Atlas (<http://mouse.brain-map.org>) were used. The framework, workflow, and equipment were previously described<sup>24</sup> and can be found at Data Production Processes in the Documentation – Supplementary Materials section of the Allen Mouse Brain Atlas (<http://mouse.brain-map.org/pdf/ABADataProductionProcesses.pdf>). Information about Cre or reporter specific probes used in ISH can be found at the Transgenic Mouse database (<http://transgenicmouse.alleninstitute.org/>).

## Double fluorescent *in situ* hybridization (DFISH)

Double fluorescent *in situ* hybridization (DFISH) was based on the CISH protocol, as described previously<sup>44</sup>. Briefly, riboprobes were labeled with either digoxigenin (DIG) or dinitrophenyl-11-UTP (DNP; Perkin Elmer). The DIG-labeled probe and DNP-labeled probe were hybridized simultaneously, and the signal from each was amplified with tyramide sequentially using either anti-DIG-HRP (Perkin Elmer) with tyramide-biotin or

anti-DNP-HRP (Perkin Elmer) with tyramide-DNP. Signal was detected by labeling of biotin or DNP with streptavidin-Alexa-Fluor 488 (Invitrogen/Molecular Probes) or anti-DNP-Alexa-Fluor 555 (Invitrogen/Molecular Probes) respectively. Slides were stained on a Leica Autostainer in a 200 ng/ml solution of DAPI (Invitrogen/Molecular Probes) buffered in TNT, and coverslipped with Hydromatrix mounting medium supplemented with 5.0% Dabco antifade (Sigma). Images were created from stitched tiles acquired on a DM6000B Leica microscope as described in Data Production Processes (<http://mouse.brain-map.org/pdf/ABADDataProductionProcesses.pdf>) except that focusing and bounding boxes were established using DAPI signal.

### **Tape transfer sectioning**

Tape transfer sectioning was done on a Leica 3050 S Cryostat equipped with an Instrumedics Tape Transfer System that includes a UV light polymerization chamber and warming pad. A roll of Instrumedics tape flags was cut into individual flags. Slides were coated with 50  $\mu$ l of Solution B adhesive and allowed to air dry. Prior to taking a section, slides were positioned on the warming pad. The tacky surface of the tape flag was positioned over the blockface of the tissue. After a section was cut and lifted on the tape flag, it was placed on the slide on the warming pad. A brush was used to apply pressure to the tape flag so that it was thoroughly laminated to the slide. After all tape flags for a slide were laminated, the slide was placed into the UV light polymerization unit, which was subsequently activated. Following UV light treatment, the tape flags were removed with forceps, leaving the sections stuck to the slide.

### **Localization of XFP and Immunohistochemistry (IHC)**

Animals were perfused with 4% paraformaldehyde in 0.1 M PB. Brains were fixed for an additional 18 hr at 4°C. Brains were then cryoprotected in 20% (w/v) sucrose in PBS at 4°C overnight. Brains were embedded in OCT and 25- $\mu$ m cryosections were cut using the tape transfer method. For direct imaging of XFP, sections were DAPI stained and coverslipped as above. For single-label immunofluorescence, sections were incubated for 30 min at room temperature in PBS containing 0.3% Triton X-100 and 5% normal goat serum (NGS). Sections were incubated with anti- GFP (Abcam; 1:1000 dilution) overnight at 4°C. Sections were rinsed for 30 min in PBS containing 1% NGS, incubated in goat anti-rabbit IgG-Alexa Fluor 488 (Invitrogen; 1:400 dilution) for 2 hr at room temperature, rinsed for 10 min in PBS containing 1% NGS, and rinsed for 30 min in PBS. Sections were then DAPI stained and coverslipped as above. XFP or IHC imaging was identical to the DFISH automated fluorescence microscopy method.

### **Confocal imaging**

Perfused brains were sectioned to 100  $\mu$ m using a Leica SM2000R sliding microtome. Sections were imaged using a BD CarvII spinning disk confocal imaging system (BD Biosciences) attached to a Leica DM6000B microscope using Leica 20x/0.70 NA, 40x/1.25 NA oil or 100x/1.4 NA oil lenses as appropriate. Images were collected using a Spot Boost EM CCD camera. Images were captured with IPLab Software (Scanalytics Inc.).

### ***In vivo* 2-photon imaging**

A custom-built 2-photon scanning microscope<sup>45</sup> with a Mai-Tai DeepSee laser (Spectra Physics) was used. Mice were anesthetized and ventilated with 0.7% isoflurane in a 20:80, O<sub>2</sub>:N<sub>2</sub> mixture and sedated using an injectible sedative, chlorprothixene (1–2 mg/kg). Through a craniotomy window the calcium indicator dye, Oregon Green BAPTA-1 (OGB), was bulk-loaded using patch pipettes into layer 2/3 of the mouse visual cortex V1<sup>46</sup>. Two different 2-photon excitation wavelengths, *i.e.* 950nm and 800nm, were used to distinguish red tdTomato labeled cells from the OGB signal, respectively. Images were acquired with a 605nm filter for tdTomato and a 525nm filter for OGB. Images were acquired at various depths (100–400 μm).

### **Cre-expressing recombinant adeno-associated virus (rAAV-Cre)**

EGFP-Cre (Addgene) was cloned into the pAAV-MCS vector (Stratagene). The resultant recombinant viral vector was packaged in the capsid of serotype 8, and high-titer virus (approximately 10<sup>13</sup> genome copy (gc)/ml) was produced by Harvard Gene Therapy Initiative (HGTI). To visualize the projections from the somatosensory cortex, 1–2 μl of rAAV-EGFP-Cre (1.6 × 10<sup>13</sup> gc/ml) was injected into anesthetized Ai14 mice at corresponding stereotaxic coordinates using a glass micropipette attached to a Picospritzer (Parker Hannifin). The virus was administered slowly by a number of low pressure air puffs to minimize tissue damage (10 psi, 10–20 ms duration, 2 Hz and 10 min/μl). Mice were then recovered and housed individually until they were utilized for further analysis.

### **RT-qPCR to quantify EYFP transcript levels**

Tissues were dissected and immediately stored in RNALater (Ambion) at 4°C until RNA isolation. RNA was isolated from homogenized tissues using the TRIzol Reagent (Invitrogen) and purified using the MagMax-96 Total RNA Isolation kit (Ambion). RNA concentration was normalized to 100 ng/μl. Equal amounts (~800 ng) of total RNA were used in each reverse transcription (RT) reaction using a SuperScript III First Strand Synthesis kit (Invitrogen) with a mixture of oligo(dT) and random primers. Each reaction was run in duplicate with reverse transcriptase (RT+) or without (RT–) to control for any potential genomic DNA contamination. Real-time qPCR was conducted using cDNA (from 1/20<sup>th</sup> of the RT reactions) with gene specific primer pairs as well as a positive control primer pair of *Gapdh*, Using SYBR Green PCR Master Mix (Roche). Each sample was run in 4 replicates, on a Roche LightCycler Real-time PCR system. On completion of a real-time qPCR experiment, thermal denaturation profile of the resulting amplicon was determined in order to make sure that the same specific amplicon is detected in different samples. Difference in number of cycles needed to reach a threshold level of fluorescence with gene-specific primers as compared with *Gapdh* primers (Cp) was used as measure of relative mRNA abundance.

### **Statistical analysis**

Expression levels were analyzed with 2-tailed Student's t-test at an alpha level of 0.05.

## Supplementary Material

Refer to Web version on PubMed Central for supplementary material.

## Acknowledgments

We are extremely grateful for the professional support of the entire Atlas Production Team, led by Paul Wohnoutka, and the Information Technology Team, led by Chinh Dang, at the Allen Institute, without which the work would have not been possible to accomplish. We are thankful to Amy Bernard for her significant contribution in establishing the DFISH process, Leonard Kuan for ISH data quantification, and Robert Hunter for coordinating transgenic mice production. We also gratefully acknowledge the following researchers for providing various research materials: Roger Tsien for the tdTomato DNA construct, Liqun Luo for the Rosa-CAG targeting construct, Karl Deisseroth for the WPRE-containing DNA construct, Brian Sauer via Addgene for the Cre and EGFP-Cre DNA constructs, Pierre Chambon for the CreERT2 DNA construct, Philippe Soriano via Addgene for the PhiC31o, FLPo and pPGKneotpAlox2 DNA constructs, Andras Nagy for the G4 ES cell line, Guillermo Oliver for the *Six3*-Cre mice, Nathaniel Heintz via Mutant Mouse Regional Resource Centers (MMRRC) for the *Ntsr1*-Cre mice, and Xiaoxi Zhuang for the *Slc6a3*-Cre mice. This work was funded by the Allen Institute for Brain Science, and an NIH grant (MH085500) to H. Zeng. The authors wish to thank the Allen Institute founders, Paul G. Allen and Jody Patton, for their vision, encouragement, and support.

## References

1. Feng G, et al. Imaging neuronal subsets in transgenic mice expressing multiple spectral variants of GFP. *Neuron*. 2000; 28:41–51. [PubMed: 11086982]
2. Sugino K, et al. Molecular taxonomy of major neuronal classes in the adult mouse forebrain. *Nature neuroscience*. 2006; 9:99–107. [PubMed: 16369481]
3. Zong H, Espinosa JS, Su HH, Muzumdar MD, Luo L. Mosaic analysis with double markers in mice. *Cell*. 2005; 121:479–492. [PubMed: 15882628]
4. Balthasar N, et al. Leptin receptor signaling in POMC neurons is required for normal body weight homeostasis. *Neuron*. 2004; 42:983–991. [PubMed: 15207242]
5. Kellendonk C, et al. Transient and selective overexpression of dopamine D2 receptors in the striatum causes persistent abnormalities in prefrontal cortex functioning. *Neuron*. 2006; 49:603–615. [PubMed: 16476668]
6. McHugh TJ, et al. *Y*. 2007; 317:94–99.
7. Karpova AY, Tervo DG, Gray NW, Svoboda K. Rapid and reversible chemical inactivation of synaptic transmission in genetically targeted neurons. *Neuron*. 2005; 48:727–735. [PubMed: 16337911]
8. Luquet S, Perez FA, Hnasko TS, Palmiter RD. NPY/AgRP neurons are essential for feeding in adult mice but can be ablated in neonates. *Science (New York, NY)*. 2005; 310:683–685.
9. Nakashiba T, Young JZ, McHugh TJ, Buhl DL, Tonegawa S. Transgenic inhibition of synaptic transmission reveals role of CA3 output in hippocampal learning. *Science (New York, NY)*. 2008; 319:1260–1264.
10. Barth AL. Visualizing circuits and systems using transgenic reporters of neural activity. *Current opinion in neurobiology*. 2007; 17:567–571. [PubMed: 18036810]
11. Luo L, Callaway EM, Svoboda K. Genetic dissection of neural circuits. *Neuron*. 2008; 57:634–660. [PubMed: 18341986]
12. Xu X, Roby KD, Callaway EM. Mouse cortical inhibitory neuron type that coexpresses somatostatin and calretinin. *The Journal of comparative neurology*. 2006; 499:144–160. [PubMed: 16958092]
13. Holtmaat A, Wilbrecht L, Knott GW, Welker E, Svoboda K. Experience-dependent and cell-type-specific spine growth in the neocortex. *Nature*. 2006; 441:979–983. [PubMed: 16791195]
14. Livet J, et al. Transgenic strategies for combinatorial expression of fluorescent proteins in the nervous system. *Nature*. 2007; 450:56–62. [PubMed: 17972876]

15. Boyden ES, Zhang F, Bamberg E, Nagel G, Deisseroth K. Millisecond-timescale, genetically targeted optical control of neural activity. *Nature neuroscience*. 2005; 8:1263–1268. [PubMed: 16116447]
16. Arenkiel BR, et al. In vivo light-induced activation of neural circuitry in transgenic mice expressing channelrhodopsin-2. *Neuron*. 2007; 54:205–218. [PubMed: 17442243]
17. Soriano P. Generalized lacZ expression with the ROSA26 Cre reporter strain. *Nature genetics*. 1999; 21:70–71. [PubMed: 9916792]
18. Srinivas S, et al. Cre reporter strains produced by targeted insertion of EYFP and ECFP into the ROSA26 locus. *BMC developmental biology*. 2001; 1:4. [PubMed: 11299042]
19. Novak A, Guo C, Yang W, Nagy A, Lobe CG. Z/EG, a double reporter mouse line that expresses enhanced green fluorescent protein upon Cre-mediated excision. *Genesis*. 2000; 28:147–155. [PubMed: 11105057]
20. Muzumdar MD, Tasic B, Miyamichi K, Li L, Luo L. A global double-fluorescent Cre reporter mouse. *Genesis*. 2007; 45:593–605. [PubMed: 17868096]
21. Shaner NC, Patterson GH, Davidson MW. Advances in fluorescent protein technology. *Journal of cell science*. 2007; 120:4247–4260. [PubMed: 18057027]
22. Zufferey R, Donello JE, Trono D, Hope TJ. Woodchuck hepatitis virus posttranscriptional regulatory element enhances expression of transgenes delivered by retroviral vectors. *Journal of virology*. 1999; 73:2886–2892. [PubMed: 10074136]
23. Raymond CS, Soriano P. High-efficiency FLP and PhiC31 site-specific recombination in mammalian cells. *PLoS ONE*. 2007; 2:e162. [PubMed: 17225864]
24. Lein ES, et al. Genome-wide atlas of gene expression in the adult mouse brain. *Nature*. 2007; 445:168–176. [PubMed: 17151600]
25. Zhuang X, Masson J, Gingrich JA, Rayport S, Hen R. Targeted gene expression in dopamine and serotonin neurons of the mouse brain. *Journal of neuroscience methods*. 2005; 143:27–32. [PubMed: 15763133]
26. Lewis PM, Gritli-Linde A, Smeyne R, Kottmann A, McMahon AP. Sonic hedgehog signaling is required for expansion of granule neuron precursors and patterning of the mouse cerebellum. *Developmental biology*. 2004; 270:393–410. [PubMed: 15183722]
27. Gong S, et al. Targeting Cre recombinase to specific neuron populations with bacterial artificial chromosome constructs. *J Neurosci*. 2007; 27:9817–9823. [PubMed: 17855595]
28. Dong, HW. *The Allen Reference Atlas: a Digital Color Brain Atlas of the C57BL/6J Male Mouse*. John Wiley & Sons; 2008.
29. Ng L, et al. Neuroinformatics for genome-wide 3D gene expression mapping in the mouse brain. *IEEE/ACM transactions on computational biology and bioinformatics / IEEE, ACM*. 2007; 4:382–393.
30. Lau C, et al. Exploration and visualization of gene expression with neuroanatomy in the adult mouse brain. *BMC bioinformatics*. 2008; 9:153. [PubMed: 18366675]
31. Coulter CL, Happe HK, Murrin LC. Postnatal development of the dopamine transporter: a quantitative autoradiographic study. *Brain research*. 1996; 92:172–181. [PubMed: 8738124]
32. Furuta Y, Lagutin O, Hogan BL, Oliver GC. Retina- and ventral forebrain-specific Cre recombinase activity in transgenic mice. *Genesis*. 2000; 26:130–132. [PubMed: 10686607]
33. Szymczak AL, et al. Correction of multi-gene deficiency in vivo using a single ‘self-cleaving’ 2A peptide-based retroviral vector. *Nature biotechnology*. 2004; 22:589–594.
34. Hippenmeyer S, et al. A developmental switch in the response of DRG neurons to ETS transcription factor signaling. *PLoS biology*. 2005; 3:e159. [PubMed: 15836427]
35. Atasoy D, Aponte Y, Su HH, Sternson SM. A FLEX switch targets Channelrhodopsin-2 to multiple cell types for imaging and long-range circuit mapping. *J Neurosci*. 2008; 28:7025–7030. [PubMed: 18614669]
36. Kuhlman SJ, Huang ZJ. High-resolution labeling and functional manipulation of specific neuron types in mouse brain by Cre-activated viral gene expression. *PLoS ONE*. 2008; 3:e2005. [PubMed: 18414675]

37. Rotolo T, Smallwood PM, Williams J, Nathans J. Genetically-directed, cell type-specific sparse labeling for the analysis of neuronal morphology. *PLoS ONE*. 2008; 3:e4099. [PubMed: 19116659]
38. Tsien JZ, et al. Subregion- and cell type-restricted gene knockout in mouse brain. *Cell*. 1996; 87:1317–1326. [PubMed: 8980237]
39. Heusner CL, Beutler LR, Houser CR, Palmiter RD. Deletion of GAD67 in dopamine receptor-1 expressing cells causes specific motor deficits. *Genesis*. 2008; 46:357–367. [PubMed: 18615733]
40. Gorski JA, et al. Cortical excitatory neurons and glia, but not GABAergic neurons, are produced in the Emx1-expressing lineage. *J Neurosci*. 2002; 22:6309–6314. [PubMed: 12151506]
41. Zhuo L, et al. hGFAP-cre transgenic mice for manipulation of glial and neuronal function in vivo. *Genesis*. 2001; 31:85–94. [PubMed: 11668683]
42. George SH, et al. Developmental and adult phenotyping directly from mutant embryonic stem cells. *Proceedings of the National Academy of Sciences of the United States of America*. 2007; 104:4455–4460. [PubMed: 17360545]
43. Zhang Y, Buchholz F, Muyrers JP, Stewart AF. A new logic for DNA engineering using recombination in *Escherichia coli*. *Nature genetics*. 1998; 20:123–128. [PubMed: 9771703]
44. Thompson CL, et al. Genomic anatomy of the hippocampus. *Neuron*. 2008; 60:1010–1021. [PubMed: 19109908]
45. Tsai, PS., et al. Principle, design and construction of a two photon laser-scanning microscope for in vitro and in vivo brain imaging. In: Frostig, RD., editor. *In vivo optical imaging of brain function*. CRC Press; 2002. p. 113-172.
46. Garaschuk O, Milos RI, Konnerth A. Targeted bulk-loading of fluorescent indicators for two-photon brain imaging in vivo. *Nature protocols*. 2006; 1:380–386. [PubMed: 17406260]

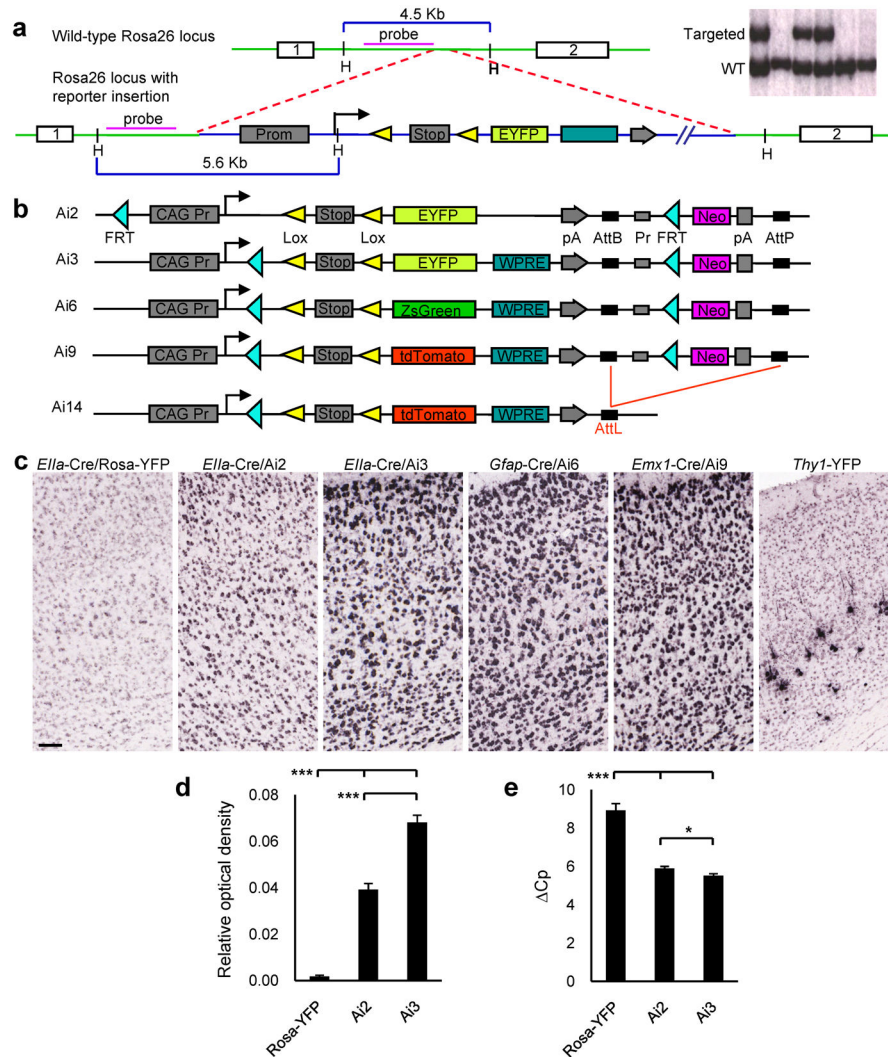


**Figure 1.** Generation of the Cre-reporter lines. **(a)** Schematic diagram of the gene targeting strategy to insert the Cre reporter cassette into the *Rosa26* locus, in the intron between endogenous exons 1 and 2. Upper right panel shows a partial Southern blot screen using *HindIII* digested genomic DNA and the probe indicated in the diagram. Full-length blot is presented in Supplementary Fig. 1 online. **(b)** Configurations of different Cre-reporter constructs inserted into the *Rosa26* locus. The PGK-Neo marker in Ai9 ES clone was deleted by transfection of a PhiC31-expressing plasmid, generating the Ai14 ES clone. **(c)** Comparison of reporter expression in the cortex between *Rosa26*-EYFP and new reporter lines. Cre lines used are indicated above each panel. Scale bar, 100  $\mu$ m. **(d)** Quantification of EYFP ISH signals in *Ella-Cre/Rosa-YFP*, *Ella-Cre/Ai2* and *Ella-Cre/Ai3* mice, with whole brain sections as AOIs. Relative optical density was measured as the IOD ratio: IOD ratio = IOD / total AOI area. IOD =  $\sum OD(p)$ , such that the optical density of individual expression object pixels are summed over the AOI. \*\*\*  $p < 0.001$  ( $n = 3$  sections per brain; Student's t-test). **(e)** Quantitative RT-PCR of EYFP using 2 sets of primer pairs on the total RNA extracted from cerebellums of *Pcp2-Cre/Rosa26-EYFP*, *Pcp2-Cre/Ai2* or *Pcp2-Cre/Ai3* mice.  $C_p = C_p$

YFP – Cp *Gapdh*. Cp, number of real-time PCR cycles. Rosa-YFP, n = 4; Ai2, n = 8; Ai3, n = 12; Student's t-test. \*\*\* p < 0.001. \* p < 0.05. Values plotted are mean ± SEM.

Author Manuscript

Author Manuscript

Author Manuscript

Author Manuscript

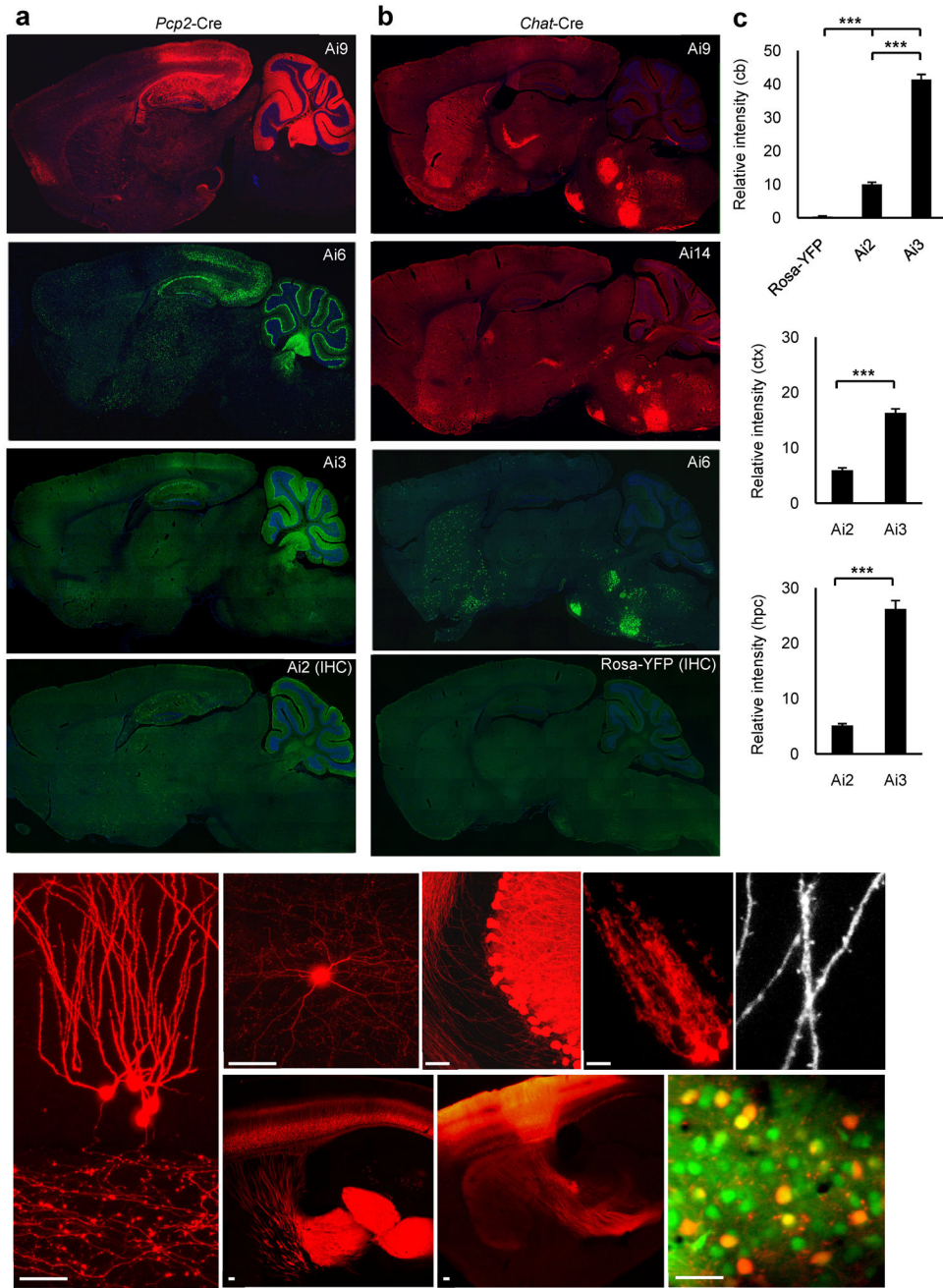


**Figure 2.** Significantly enhanced fluorescent labeling in the new reporter lines. **(a–b)** Comparison of fluorescence in various reporter lines crossed to the same Cre-driver line: *Pcp2-Cre* in (a), and *Chat-Cre* in (b). IHC indicates immunostaining using anti-GFP. Unlike tdTomato fluorescence which was also visible in axonal projections, ZsGreen fluorescence was mostly confined to the cell bodies. Scale bar, 500  $\mu$ m. **(c)** Quantification of fluorescence in single neurons of *Pcp2-Cre/Rosa26-EYFP*, *Pcp2-Cre/Ai2* or *Pcp2-Cre/Ai3* mice, on section images with 140-ms exposure time (no saturation). Three types of neurons were quantified, cerebellar Purkinje cells (cb, upper panel), cortical neurons (ctx, middle panel), and

hippocampal CA1 pyramidal neurons (hpc, lower panel). Relative intensity = intensity of the object (cell) – intensity of the background. For each of Ai2 and Ai3, n = 30 randomly selected neurons from 3 sections per region. For Rosa-YFP, only n = 10 randomly selected neurons from one section was used in the Purkinje cell quantification, due to undetectability in the other two. \*\*\* p < 0.001. Values plotted are mean ± SEM. **(d–h)** Distinctive morphologies of various cell types labeled by tdTomato: (d) dentate granule cells; (e) a cortical interneuron; (f) Purkinje cells; (g) cerebellar Bergmann glia cells; (h) dendritic spines. **(i)** Corticothalamic projections from cortical layer 6 neurons in *Ntsr1*-Cre/Ai14 mice. **(j)** Corticothalamic projections in an Ai14 mouse with rAAV-Cre injected into the somatosensory cortex. **(k)** *In vivo* 2-photon imaging of tdTomato expressing neurons (red) and OGB-loaded neurons (green) in visual cortical layer 2/3 of an anesthetized *Wfs1*-Tg2-CreERT2/Ai9 mouse. Scale bar, 50 μm.

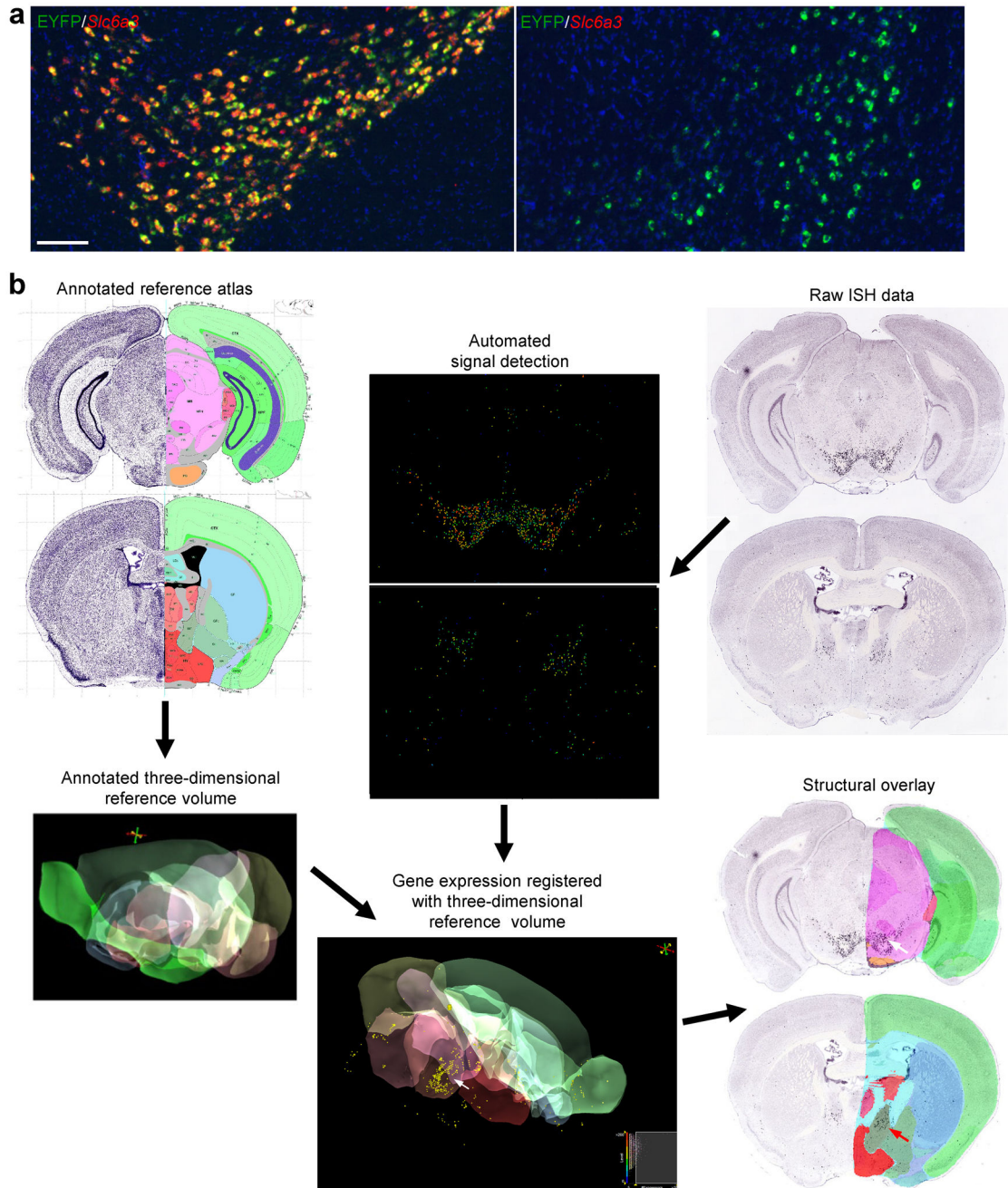


**Figure 3.** Informatics processing of the ISH characterization data. **(a)** Co-labeling of EYFP (green) with *Slc6a3* (red) in the *Slc6a3*-Cre/Ai3 mouse by DFISH. In the VTA/substantia nigra region (left panel), EYFP was largely co-localized with *Slc6a3* (>90% cells were co-labeled), demonstrating expected Cre-recombination in dopamine neurons. In the basal forebrain area (right panel), the cluster of EYFP-positive cells were *Slc6a3*-negative. Scale bar, 200  $\mu$ m. **(b)** EYFP ISH data from a *Slc6a3*-Cre/Ai3 mouse were digitized and registered to the Allen Reference Atlas, which allows anatomical search and comparison. Two sections

of registered EYFP ISH data are shown overlaid with anatomical partitioning. EYFP expression is present in both sections (white and red arrows).

Author Manuscript

Author Manuscript

Author Manuscript

Author Manuscript

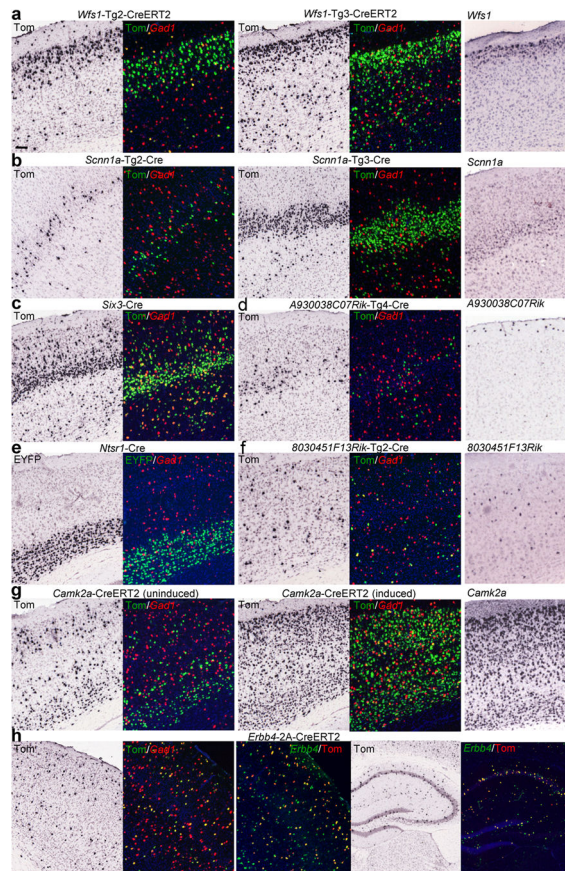


**Figure 4.**

New Cre lines and their differential recombination patterns in different cortical cell types. For each Cre line, both CISH of the reporter gene (tdTomato (Tom) or EYFP) and DFISH of the reporter (green) with *Gad1* (red) are shown for the cortex only. CISH of some of the endogenous genes used to make Cre lines is also shown in the rightmost panel. The mice used are: (a) *Wfs1*-Tg2-CreERT2/Ai9 and *Wfs1*-Tg3-CreERT2/Ai9 with tamoxifen induction. (b) *Scnn1a*-Tg2-Cre/Ai9 and *Scnn1a*-Tg3-Cre/Ai9. (c) *Six3*-Cre/Ai9. (d) *A930038C07Rik*-Tg4-Cre/Ai9. (e) *Ntsr1*-Cre/Ai3. (f) *8030451F13Rik*-Tg2-Cre/Ai9. (g) *Camk2a*-CreERT2/Ai14 without or with tamoxifen induction. (h) *ErbB4-2A*-CreERT2/Ai14 with tamoxifen induction, shown for both cortex and hippocampus to demonstrate the scattered population of interneurons. DFISH of *ErbB4* (green) with tdTomato (red) shows the faithful but incomplete recapitulation of recombination in *ErbB4* positive cells. DAPI staining is shown in blue. Scale bar, 100  $\mu$ m.

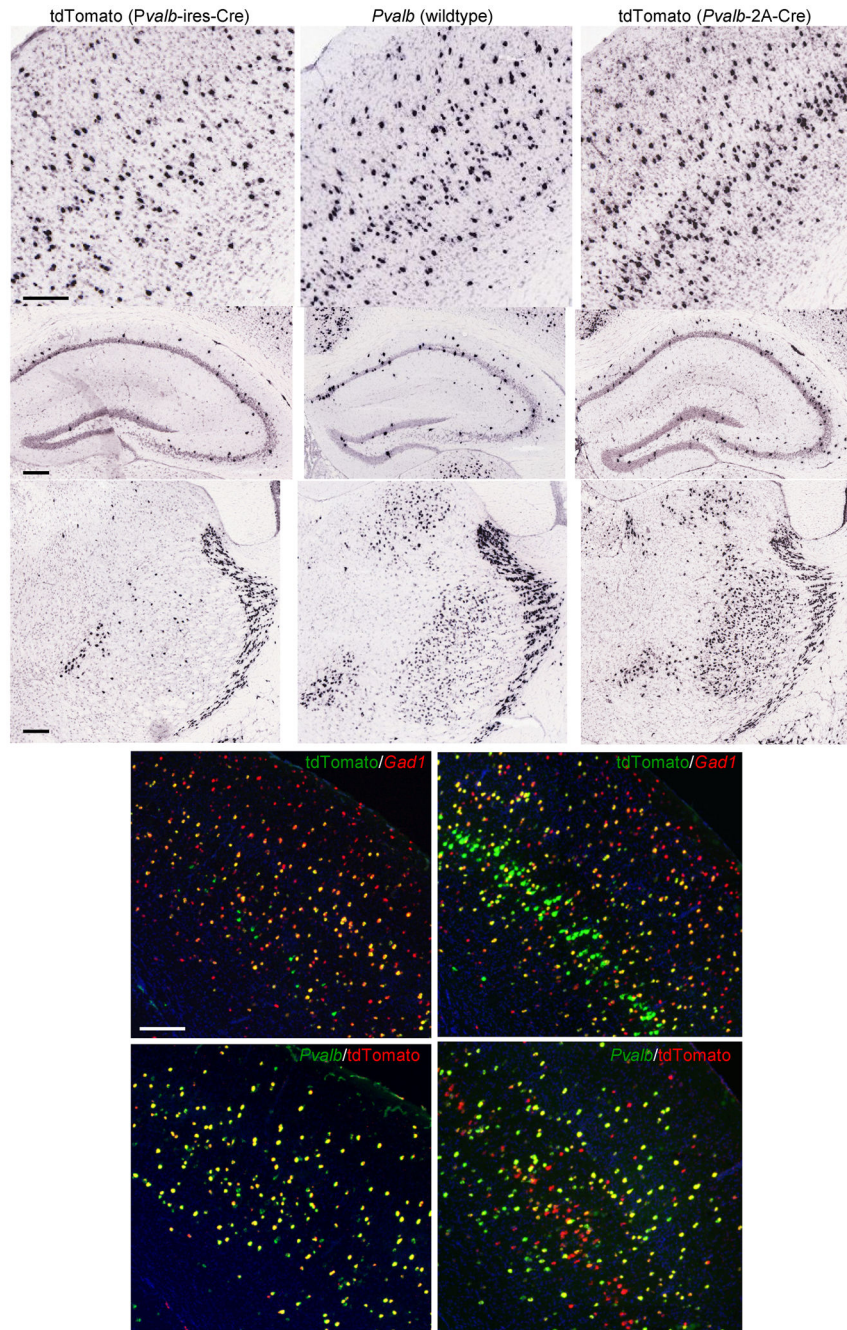


**Figure 5.** Comparison of recombination patterns in two closely related knock-in Cre lines, *Pvalb-ires-Cre* and *Pvalb-2A-Cre*. (a–i) CISH comparison of tdTomato reporter in *Pvalb-ires-Cre*/Ai14 mouse (left panels: a, d, g), the endogenous *Pvalb* gene (middle panels: b, e, h), and tdTomato reporter in *Pvalb-2A-Cre*/Ai14 mouse (right panels: c, f, i) in 3 areas of the brain: cortex (top panels: a, b, c), hippocampus (middle panels: d, e, f) and thalamus (bottom panels: g, h, i). (j–k) DFISH comparison of tdTomato (green) with Gad1 (red) between

Pvalb-ires-Cre (j) and Pvalb-2A-Cre (k). **(l-m)** DFISH comparison of Pvalb (green) with tdTomato (red) between Pvalb-ires-Cre (l) and Pvalb-2A-Cre (m). Scale bar, 200  $\mu$ m.

Author Manuscript

Author Manuscript

Author Manuscript

Author Manuscript

Table 1

Cre driver lines that have been characterized

Cre line*	Reporter	CISH data	DFISH data	XFP data	Expression highlight#	JAX or MMRRC #
803045/ <i>F13Rik-Tg2-Cre</i>	Ai9	tdTomato, Cre	tdTomato/Gad1	tdTomato	Scattered populations in the cortex and hippocampus	JAX #008848
	Ai2			EYFP		
<i>A93003807Rik-Tg4-Cre</i>	Ai9	tdTomato, Cre	tdTomato/Gad1	tdTomato	Scattered populations enriched in layers 3/4/5	JAX #009616
	Ai2	EYFP, Cre	EYFP/Gad1	EYFP	Widespread in forebrain areas, e.g. cortex, hippocampus, striatum	JAX #005359
<i>Camk2a-Cre</i> <sup>38</sup>	Ai9	tdTomato	tdTomato/Gad1	tdTomato		
	Ai14	tdTomato	tdTomato/Gad1	tdTomato	Scattered populations in cortex	
<i>Camk2a-CreERT2</i> (uninduced) §	Ai6			ZsGreen		
	Ai14	tdTomato	tdTomato/Gad1	tdTomato	Widespread in forebrain areas, e.g. cortex, hippocampus, striatum	
<i>Camk2a-CreERT2</i> (induced) §	Ai6			ZsGreen		
	Ai9	tdTomato, Cre	tdTomato/Chat, tdTomato/Gad1	tdTomato	Cholinergic neurons	JAX #006410
<i>Chat-Cre</i>	Ai6			ZsGreen		
	Ai3	EYFP, Cre	EYFP/Gad1, EYFP/Drd1a	EYFP	Striatum and cortex	
<i>Drd1a-Cre</i> <sup>39</sup>	Ai9	tdTomato		tdTomato		
	Ai9	tdTomato, Cre	tdTomato/Gad1, Emx1/tdTomato	tdTomato	Widespread in cortex	JAX #005628
<i>Emx1-ires-Cre</i> <sup>40</sup>	Ai14	tdTomato, Cre	tdTomato/Gad1, Pvalb/tdTomato, ErbB4/tdTomato	tdTomato	Scattered interneuron populations in cortex, hippocampus	
	Ai3	EYFP	Gfap/EYFP		Both astrocytes and widespread neuronal expression	JAX #004600
<i>Gfap-Cre</i> <sup>41</sup>	Ai6	ZsGreen, Cre	Gfap/ZsGreen	ZsGreen		
	Ai3	EYFP	EYFP/Gad1	EYFP	Layer 6 specific	MMRRC #017266
<i>Nes1-Cre</i> <sup>27</sup>	Ai14	tdTomato	tdTomato/Gad1	tdTomato		
	Ai14	tdTomato	tdTomato/Gad1, Pvalb/tdTomato	tdTomato	Pvalbumin-positive interneurons and excitatory neurons in layer 5	
<i>Pvalb-2A-Cre</i>	Ai9	tdTomato, Cre	tdTomato/Gad1, Pvalb/tdTomato	tdTomato		
	Ai14	tdTomato, Cre	tdTomato/Gad1, Pvalb/tdTomato	tdTomato	Pvalbumin-positive interneurons	JAX #008069
<i>Pvalb-ires-Cre</i> <sup>34</sup>	Ai9	tdTomato	tdTomato/Gad1, Pvalb/tdTomato	tdTomato		
	Ai2	EYFP	Pcp2/EYFP	EYFP	Purkinje cells, scattered population of cells (glial) throughout the brain, also	JAX #006207
<i>Pcp2-Cre</i> <sup>26</sup>	Ai9	tdTomato	Pcp2/tdTomato	tdTomato		

Cre line*	Reporter	CISH data	DFISH data	XFP data	Expression highlight#	JAX or MMRRC #
	Ai6	ZsGreen, Cre		ZsGreen	enriched neuronal expression in visual cortex	
	Ai3	EYFP		EYFP		
<i>Pomc</i> -Cre <sup>4</sup>	Ai3	EYFP, Cre	EYFP/Pomc1	EYFP	POMC-positive neurons in hypothalamus, also in dentate gyrus	JAX #005965
	Ai9			tdTomato		
<i>Scnn1a</i> - <b>Tg1</b> -Cre	Ai9	tdTomato, Cre	tdTomato/Gad1	tdTomato	Enriched in layer 4, plus scattered widespread expression	JAX #009111
<i>Scnn1a</i> - <b>Tg2</b> -Cre	Ai9	tdTomato, Cre	tdTomato/Gad1	tdTomato	Very sparse cells in layer 4, mostly in somatosensory area	JAX #009112
<i>Scnn1a</i> - <b>Tg3</b> -Cre	Ai9	tdTomato, Cre	tdTomato/Gad1	tdTomato	Layer 4 specific	JAX #009613
<i>Six3</i> -Cre <sup>32</sup>	Ai3	EYFP	EYFP/Gad1	EYFP	Enriched in layer 4, plus scattered populations in cortex, striatum	
	Ai9	tdTomato	tdTomato/Gad1	tdTomato		
<i>Slc6a3</i> -Cre <sup>25</sup>	Ai3	EYFP, Cre	EYFP/Slc6a3	EYFP	Dopamine neurons, plus sparse populations elsewhere	
	Ai9	tdTomato	Slc6a3/tdTomato	tdTomato		
<i>Wfs1</i> - <b>Tg2</b> - <b>CreERT2</b> (induced) §	Ai9	tdTomato, Cre	tdTomato/Gad1	tdTomato	Enriched in layers 2/3	JAX #009614
<i>Wfs1</i> - <b>Tg3</b> - <b>CreERT2</b> (induced) §	Ai9	tdTomato, Cre	tdTomato/Gad1	tdTomato	Enriched in layers 2/3 plus scattered populations in cortex	JAX #009103

\* Cre lines in bold are newly generated lines.

# Expression highlights describe only the most relevant cell populations targeted by the Cre lines, not including all the cell populations where Cre-recombination occurs.

§ Induced or uninduced refers to with or without tamoxifen treatment for CreERT2-containing mice.